The RCK1 domain of the human BK_{Ca} channel transduces Ca^{2+} binding into structural rearrangements

Taleh Yusifov,[1] Anoosh D. Javaherian,[1] Antonios Pantazis,[1] Chris S. Gandhi,[4] and Riccardo Olcese[1,2,3]

[1]Division of Molecular Medicine, Department of Anesthesiology, [2]Cardiovascular Research Laboratory, and [3]Brain Research Institute, David Geffen School of Medicine at University of California, Los Angeles, CA 90095
[4]Division of Chemistry and Chemical Engineering, California Institute of Technology, Pasadena, CA 91125

Large-conductance voltage- and Ca^{2+}-activated K^+ (BK_{Ca}) channels play a fundamental role in cellular function by integrating information from their voltage and Ca^{2+} sensors to control membrane potential and Ca^{2+} homeostasis. The molecular mechanism of Ca^{2+}-dependent regulation of BK_{Ca} channels is unknown, but likely relies on the operation of two cytosolic domains, regulator of K^+ conductance (RCK)1 and RCK2. Using solution-based investigations, we demonstrate that the purified BK_{Ca} RCK1 domain adopts an α/β fold, binds Ca^{2+}, and assembles into an octameric superstructure similar to prokaryotic RCK domains. Results from steady-state and time-resolved spectroscopy reveal Ca^{2+}-induced conformational changes in physiologically relevant [Ca^{2+}]. The neutralization of residues known to be involved in high-affinity Ca^{2+} sensing (D362 and D367) prevented Ca^{2+}-induced structural transitions in RCK1 but did not abolish Ca^{2+} binding. We provide evidence that the RCK1 domain is a high-affinity Ca^{2+} sensor that transduces Ca^{2+} binding into structural rearrangements, likely representing elementary steps in the Ca^{2+}-dependent activation of human BK_{Ca} channels.

The Journal of General Physiology

INTRODUCTION

Ca^{2+} plays a central role as a ubiquitous signaling molecule in fundamental physiological processes and can directly or indirectly modulate the activity of a large number of proteins (Clapham, 1995; Carafoli and Klee, 1999), including several families of ion channels. In some cases, ion channels acquire Ca^{2+} sensitivity by associating with Ca^{2+}-binding proteins, such as calmodulin, that in turn modulate channel properties (Pitt, 2007). In contrast, the large-conductance voltage- and Ca^{2+}-activated K^+ (BK_{Ca} or MaxiK) channels (Marty, 1981; Pallotta et al., 1981; Latorre et al., 1982), which regulate a multitude of physiological processes including smooth muscle tone, uresis, immunity, and neurotransmission (Tang et al., 2004b; Lu et al., 2006; Salkoff et al., 2006; Cui et al., 2009), appear to be directly modulated by intracellular Ca^{2+} that binds to specialized intracellular modules known as regulator of K^+ conductance (RCK) domains (Pico, 2003; Niu et al., 2004; Lingle, 2007; Yusifov et al., 2008; Yuan et al., 2010; Wu et al., 2010).

It has been proposed that RCK domains operate as chemo-mechanical transducers that convert the free energy of Ca^{2+} binding (or other ligands) into mechanical work that ultimately opens the channel pore (Jiang et al., 2001, 2002; Niu et al., 2004; Chakrapani and Perozo, 2007). Significant insights into the structure and function of these domains were provided by crystallographic data of bacterial RCKs (Jiang et al., 2001, 2002). Sequence analysis suggests that two tandem regions of the large cytoplasmic domain of eukaryotic BK_{Ca} channels' protein conformation, RCK1 and RCK2, are structurally homologous to bacterial RCK domains (Jiang et al., 2002; Pico, 2003; Roosild et al., 2004; Fodor and Aldrich, 2006, 2009; Kim et al., 2006, 2008; Latorre and Brauchi, 2006; Yusifov et al., 2008). Indeed, the large BK_{Ca} cytosolic C terminus, recently visualized at 17–20-Å resolution by cryo-electron microscopy (Wang and Sigworth, 2009), is thought to comprise a hetero-octameric assembly of RCK1 and RCK2 domains akin to the gating ring of prokaryotic channels. This view is supported by two recent studies that report on the atomic structure of the cytoplasmic domain of the BK_{Ca} channel (Wu et al., 2010; Yuan et al., 2010). Tandem RCK1 and RCK2 domains interact with each other within the same subunit; these four RCK1/RCK2 pairs assemble in a gating ring structure through "assembly" interfaces (Wu et al., 2010; Yuan et al., 2010).

RCK domains in BK_{Ca} channels are thought to be involved in high-affinity Ca^{2+} sensing (Niu et al., 2004; Latorre and Brauchi, 2006; Qian et al., 2006; Lingle,

Correspondence to Riccardo Olcese: rolcese@ucla.edu

Abbreviations used in this paper: BK_{Ca}, large-conductance voltage- and Ca^{2+}-activated K^+; CD, circular dichroism; GST, glutathione *S*-transferase; MALLS, multi-angle laser light scattering; RCK, regulator of K^+ conductance; WT, wild type.

The Rockefeller University Press $30.00
J. Gen. Physiol. Vol. 136 No. 2 189–202
www.jgp.org/cgi/doi/10.1085/jgp.200910374

2007; Yusifov et al., 2008). In the RCK2 domain, high-affinity Ca^{2+} sensing is endowed by a Ca^{2+}-binding region termed the "Ca^{2+} bowl" consisting of five consecutive aspartates (894–898) (Schreiber and Salkoff, 1997; Schreiber et al., 1999), which are critical for Ca^{2+} binding (Bian et al., 2001; Braun and Sy, 2001; Bao et al., 2004; Sheng et al., 2005; Yuan et al., 2010) and Ca^{2+}-induced conformational changes (Yusifov et al., 2008). In RCK1, mutations of aspartates 362/367 or methionine 513 reduce the high-affinity Ca^{2+} sensitivity of the channel (Bao et al., 2002; Xia et al., 2002; Zeng et al., 2005; Sweet and Cox, 2008). Indeed, the concomitant neutralization of D362/367 (RCK1) and the Ca^{2+} bowl (RCK2) to alanine residues completely abolishes the high-affinity Ca^{2+} dependence of BK_{Ca} channels (Xia et al., 2002; Zeng et al., 2005; Sweet and Cox, 2008). However, no Ca^{2+}-binding sites within the RCK1 domain have yet been observed (Wu et al., 2010; Yuan et al., 2010). Thus, the molecular details of Ca^{2+} sensing in the RCK1 domain remain unknown.

To shed light on the molecular basis for Ca^{2+}-dependent channel activation, we have expressed and purified the cytosolic part of the BK_{Ca} channel corresponding to the RCK1 region and interrogated its function as a Ca^{2+} sensor, as previously performed for the RCK2 domain (Yusifov et al., 2008). We postulate that a Ca^{2+} sensor involved in the Ca^{2+}-dependent activation of the channel must satisfy the following criteria: bind Ca^{2+}; undergo Ca^{2+}-dependent conformational transitions (to exert mechanical force to open the pore); operate in a physiologically relevant range of $[Ca^{2+}]$; and, finally, mutations of critical residues involved in Ca^{2+}-dependent channel activation should perturb either Ca^{2+} binding, the transduction mechanism, or both. We have used a combination of optical and biochemical methods to test these criteria for the RCK1 domain of the human BK_{Ca} (Slo1) channel.

MATERIALS AND METHODS

Expression and purification of the human BK_{Ca} RCK1 and RCK2 domains

Expression and site-directed mutagenesis of the human Slo1 RCK1 domain with flanking N- and C-terminal regions (^{322}IIE...HDP^{667}) and the BK_{Ca} RCK2 domain (^{665}HDP...ALK^{1005}) were performed as described previously (Yusifov et al., 2008). The protein fractions were solubilized in 50 mM Tris-HCl and 8 M urea, pH 8.0. The supernatant was refolded by dialysis to 50 mM Tris and 2 mM EGTA, pH 7.5, and applied to a Ni-NTA affinity column. The protein fractions were eluted with 250 mM imidazole and dialyzed against 25 mM MOPS, 2 mM EGTA, and 120 mM KCl, pH 7.2. The purity of the expressed proteins was analyzed using a 12.5% SDS-PAGE. Protein concentrations were determined using the Biuret-Lowry assay.

Size-exclusion chromatography

The purified BK_{Ca} RCK1 or RCK2 domains were solubilized in 8 M urea. 500 µl of each sample was refolded onto a Superdex 200 10/300 column with a flow rate of 0.5 ml/min, equilibrated with a buffer containing 50 mM Tris and 5 mM EGTA, pH 8.4, or 20 mM MOPS and 2 mM EGTA, pH 7.2. The refolded protein fractions eluted between 10 and 11 ml were collected and reinjected into the sizing column and eluted in equilibrium buffer. The apparent mol wt of RCK1 and RCK2 was determined by constructing a calibration plot from the elution profiles of protein standards of known mol wt (MWGF1000; Sigma-Aldrich).

Multi-angle laser light scattering (MALLS)

MALLS experiments were performed with a DAWN-EOS MALLS detector coupled to an Optilab refractometer (Wyatt Technologies) and a UV-absorption spectrophotometer. The purified RCK1 domain (100 µl; 0.1 mg/ml) in 25 mM MOPS, 2 mM EGTA, and 120 mM KCl, pH 7.2, was loaded onto a QC-PAK GFC 300 column (Tosoh Bioscience). Light-scattering data were acquired from 14 detectors (detectors 1–4 were disabled, as they are unreliable for aqueous solutions) and fit by the following equation based on the Zimm formalism, using the Astra 5.3.4 program (Wyatt Technologies):

$$(K^{*}c)/R(\theta) = 1/[MW \times P(\theta)],$$

where K^{*} is an optical parameter equal to $4\pi^2 n^2 (dn/dc)^2/(\lambda_0^4 N_A)$, where n is the solvent refractive index, dn/dc is the refractive index increment (0.185), λ is the wavelength of the scattered light in vacuum (cm), and N_A is Avogadro's number. Parameter c is the sample concentration in g/ml, $R(\theta)$ is the excess intensity of scattered light at DAWN angle θ, MW is the weighted-average mol wt, and $P(\theta)$ describes the angular dependence of the scattered light. The proportion of eluted protein, determined by UV absorption at 280 nm, was binned according to mol wt, as determined by light scatter analysis.

Circular dichroism (CD) spectroscopy

CD spectra and free $[Ca^{2+}]$ were obtained as described previously (Yusifov et al., 2008). CD data are presented in units of molar ellipticity per residue. Computational analysis of the far-UV CD spectra of the purified proteins was done using the SELCON3 algorithm of the CDPro software package (Sreerama and Woody, 2004). Secondary structure composition was estimated using SMP56 (IBasis 10). Normalized root mean-square deviation is defined as

$$\left[\sum(\theta_{\exp}-\theta_{cal})^2 / \sum(\theta_{\exp})^2\right]^{1/2},$$

where $\theta_{\exp}$ and θ_{cal} is the experimental and calculated molar ellipticity per amino acid residue, respectively. The number of the α-helix secondary structure segments (n_α) was calculated by dividing the number of residues included in the distorted α-helix structure by a factor of four and in the distorted β structure (n_β) by a factor of two.

Time-resolved fluorescence

The time-resolved fluorescence decay of endogenous tryptophan was recorded with a spectrofluorometer (Fluorolog-3; HORIBA) using the time-correlated single-photon counting method at 22°C with a pulsed nanoLED at λ_{ex} = 296 nm. Ludox was used as scatter solution. The fluorescence intensity decay data were fit with a sum of three exponential functions, using the DAS6 v6.4 software (HORIBA):

$$I(t) = \sum_{i=1}^{n} \alpha_i \exp(-t/\tau_i),$$

where I is the fluorescence intensity and α_i and τ_i are the normalized preexponential factors and decay times, respectively. The average fluorescence lifetimes (τ_{avg}) for three exponential iterative fittings

are calculated from the decay times and preexponential factors using equations

$$\tau_{avg} = \sum_{i-1}^{n} f_i t_i,$$

where f_i shows the fractional contribution of each decay time to the steady-state intensity, which is given by

$$f_i = \alpha_i \tau_i / \sum \alpha_j \tau_j.$$

The goodness of the fit was determined from its χ^2 value and the variance of the weighted residual distribution.

Steady-state fluorescence

Intrinsic tryptophan fluorescence spectra were recorded with protein concentrations of 0.1 mg/ml in 25 mM MOPS, 2 mM EGTA, and 120 mM KCl, pH 7.2. Fluorescence measurements were obtained using excitation/emission slit widths of 5 nm each, with λ_{ex} = 295 nm. The tryptophan emission fluorescence spectra were collected in the wavelength range of 300–400 nm. Experiments were fit with a Hill function in the form:

$$F_{330} = \left(F_{max} - F_{min}\right) / \left(1 + \left(\left[Ca^{2+}\right]\right) / K_{1/2}\right)^{n} + F_{min}.$$

$^{45}Ca^{2+}$-binding assay

Purified wild-type (WT) and D362/367A-RCK1 (30 µg each) were centrifuged at 13,000 rpm for 5 min and then blotted onto nitrocellulose membranes prestained with 0.1% Ponceau S and 5% acetic acid (Morçöl and Subramanian, 1999). 10 µg troponin and 10 µg glutathione *S*-transferase (GST) were used as positive and negative controls, respectively. After protein blotting, the membranes were stained again with Ponceau S and washed five times with distilled water to remove nonspecific staining and estimate the relative protein abundance. The membranes were then probed by $^{45}Ca^{2+}$ overlay as reported previously (Levitsky et al., 1994). In brief, the membranes were placed in a wash solution containing 60 mM KCl, 10 mM imidazole, and 2 mM $MgCl_2$, pH 7.2, for 30 min, followed by a 60-min wash in the same solution supplemented with 115 µM $CaCl_2$, and different concentrations of EGTA to obtain the desired free [Ca^{2+}]. Then, 6 µC/ml $^{45}Ca^{2+}$ (PerkinElmer) was added to this solution, and the membrane was washed for an additional 10 min. The free [Ca^{2+}] was estimated with WebMaxC and measured with a Ca^{2+}-selective electrode (WPI) or by using a calibration curve constructed from the fluorescent Ca^{2+}-sensitive Ca^{2+} green 5N dye (Takahashi et al., 1999). The membranes were then washed twice in distilled water, dried, and exposed to a phosphor storage screen for 1–3 d. Relative binding was obtained by dividing the pixel values of the $^{45}Ca^{2+}$ signal of each protein by the pixel values of its Ponceau S staining using the ImageJ 1.43S program (http://rsb.info.nih.gov/ij/).

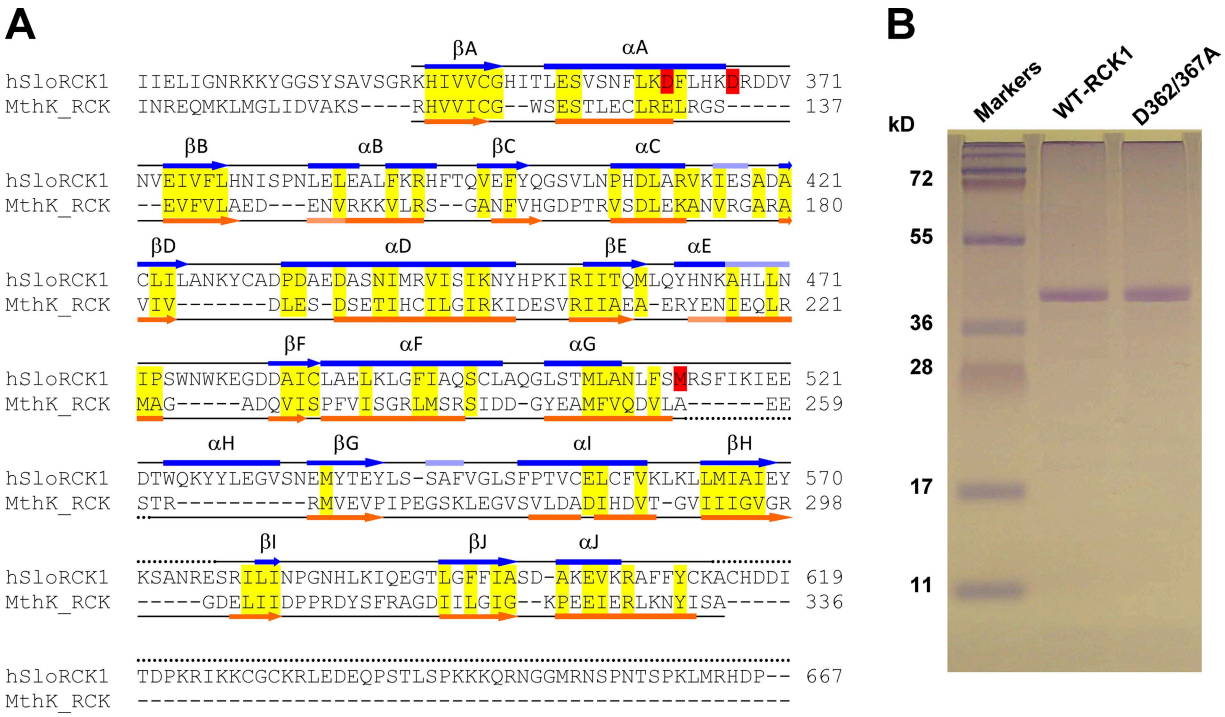

Figure 1. Purification of the RCK1 domain of the human BK_{Ca} channel. (A) Structure-based sequence alignment of the BK_{Ca} channel (GI, 507922) C terminus (encompassing the RCK1 domain) with the MthK (GI, 2622639) RCK domain. The α helices are depicted as bars, and β strands are shown as arrows. The secondary structures (obtained from the DSSP reference set) above the sequences (blue) are obtained from the atomic structure of the BK_{Ca} C-terminal domain (Protein Data Bank accession no. 3MT5) (Yuan et al., 2010) and below the sequences (orange) are obtained from the atomic structure of the MthK RCK domain (Protein Data Bank accession no. 2AEF) (Dong et al., 2005). Light blue and light orange bars correspond to 3_{10} helices. Dotted lines are unresolved regions in the respective crystal structures. Semi-conserved residues within ordered structures are highlighted yellow. Residues known to be involved in high-affinity Ca^{2+} sensitivity in the BK_{Ca} RCK1 domain (D362/D367 and M513) are highlighted red. (B) 12.5% SDS-PAGE of purified WT-RCK1 and D362/367A-RCK1 stained with Coomassie blue. Both proteins migrate as an ∼40-kD band, consistent with their expected mol wt (41 kD).

Cleavage of N-terminal 6xHis tag of the purified WT-RCK1 domain was performed using the TAGZyme system (QIAGEN). In brief, 50 µg RCK1 was incubated in the presence of 5 U/ml dipeptidyl aminopeptidase I (DAPase) enzyme mixed with 2 mM cysteamine-HCl (QIAGEN) for several time intervals at 37°C. Reaction efficiency of 6xHis tag cleavage was analyzed using InVision His tag in-gel stain (Invitrogen). The WT-RCK1 domain lacking the 6xHis tag was separated from undigested 6xHis-tagged RCK1 and DAPase using NI-NTA immobilized metal affinity chromatography (IMAC; QIAGEN).

RESULTS

Expression and purification of the C terminus region of the human BK_{Ca} channel corresponding to the RCK1 domain

To directly investigate the structure and Ca^{2+}-sensing properties of the human BK_{Ca} RCK1 domain in solution, we expressed and purified the region of the human BK_{Ca} channel C terminus corresponding to the amino acid sequence ^{322}IIE...HDP^{667} (Wallner et al., 1995), which includes the S6-RCK1 linker (^{322}IIE...GRK^{343}), the RCK1 domain (^{344}HIV...FYC^{612}), and part of the RCK1-RCK2 interconnecting linker (^{613}KAC...HDP^{667}) (Yuan et al., 2010). In spite of the poor amino acid sequence similarity between the BK_{Ca} channel RCK1 domain and the MthK RCK domain (<25%), they share structural similarities (Fig. 1 A).

We also expressed and purified a RCK1 mutant carrying the D362A/367A mutations to probe the role of these residues, which are known to be critical for high-affinity Ca^{2+} sensitivity (Xia et al., 2002; Zeng et al., 2005; Sweet and Cox, 2008). The purity of the two proteins was assessed by SDS-PAGE. The WT and D362/367A-RCK1 domains both migrate as a 40-kD band in denaturating conditions, close to their theoretical mol wt of a monomeric RCK1 domain (41 kD; Fig. 1 B).

The secondary and quaternary structures of the RCK1 domain in solution share similarities with bacterial RCK domains

The secondary structure of the purified RCK1 domain was probed by CD spectroscopy, a powerful technique for the determination of secondary structure composition and ligand-induced conformational changes of proteins in solution (Kelly et al., 2005; Greenfield, 2006). The far-UV CD spectrum of WT-RCK1 in nominal Ca^{2+} (free [Ca^{2+}] = 0.00058 µM) is presented in Fig. 2 A. The CD spectrum of WT-RCK1 shows an inflection at 210 nm and a minimum at 220 nm, characteristic of significant α-helical content (Sreerama and Woody, 2004; Turk et al., 2006). The analysis of the CD spectrum of WT-RCK1 in solution suggests a secondary structure composition of ∼28% α helix and ∼23% β strand, organized in ∼10 α helices and ∼15 β strands. RCK1's folding pattern, analyzed using the cluster algorithm (Sreerama et al., 2001), revealed an α/β fold (in a consecutive β–α–β pattern; Table I), a common structural motif of the Rossmann fold (Rao and Rossmann, 1973), and an important structural feature of the RCK domains (Jiang et al., 2001, 2002; Wu et al., 2010; Yuan et al., 2010).

The oligomeric state of the purified RCK1 domain was investigated using size-exclusion chromatography. Fig. 2 B shows the elution profile of purified RCK1 on a Superdex 200 10/300 column. The elution peak (10.4 ± 0.08 ml; n = 7 elutions; errors represent standard errors of the mean) correlates to an apparent mol wt of 341 ± 10.0 kD, very close to the expected mol wt of a RCK1 octamer (theoretical RCK1 × 8 = 328 kD), according to a calibration curve constructed with protein standards of known mol wt (Fig. 2 C). These data suggest that the WT-RCK1 domain in solution preferentially self-assembles into octamers. A MALLS analysis (Wen et al., 1996;

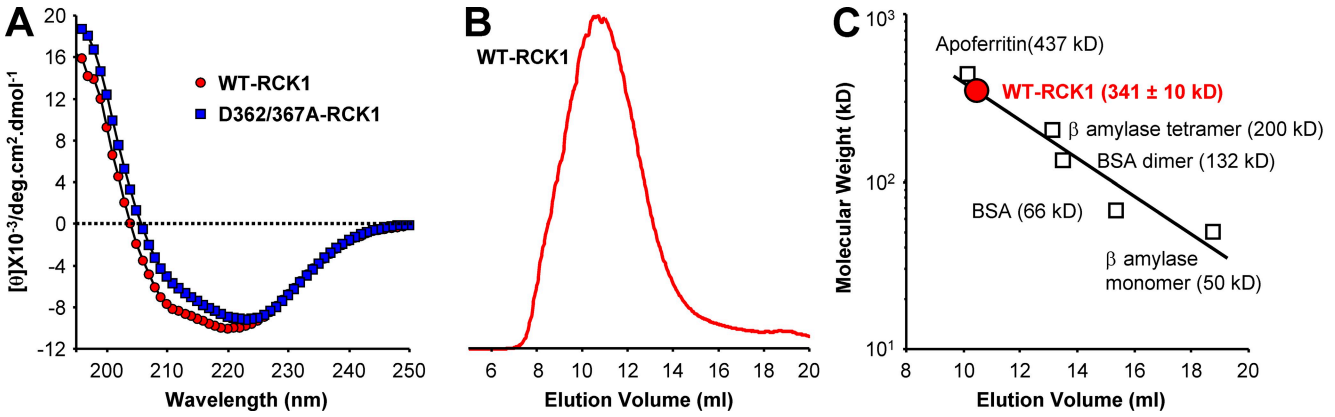

Figure 2. Structural analysis of WT and D362/367A RCK1. (A) Far-UV CD spectra of WT-RCK1 and D362/367A-RCK1 domains obtained in nominal free [Ca^{2+}] (0.00058 µM). The CD spectrum of WT-RCK1 exhibits a strong signal at 220 nm, whereas D362/367A displays different spectral properties with a red-shifted minimum at 223 nm (relative to WT-RCK1), suggesting that the double D362/367A mutation altered its secondary structure. (B) Characteristic size-exclusion column profile of the purified WT-RCK1 domain reveals an elution peak at ∼10.5 ml. (C) A calibration curve is established by plotting the log (mol wt) of proteins with known mol wt versus their elution peak (R^2 = 0.91). The purified WT-RCK1 domain is calculated to elute with an apparent mol wt of 341 ± 10.0 kD (n = 7), suggesting a homo-octameric assembly of RCK1 domains (theoretical octameric mol wt = 328 kD).

TABLE I

Estimated secondary structure composition of RCK domains

	CD spectroscopy			X-ray diffraction		
	BK_{Ca} RCK1, 0 Ca^{2+}	BK_{Ca} RCK1, 35 µM Ca^{2+}	BK_{Ca} RCK1-D362/367A	BK_{Ca} RCK1	MthK RCK	MthK RCK Ca^{2+} bound
Amino acids		^{322}IIE…HDP^{667}, 346 aa		^{343}KHI…IEY^{570}, ^{577}SRI…YCK^{613}, 265 aa	^{116}RHV...ISA^{336}, 221 aa	
Reference		This study		Yuan et al., 2010	Ye et al., 2006	Jiang et al., 2002
α helix (%)	28.1 ± 0.751	19.3 ± 0.557	24.8 ± 0.0882	39.6 (30)	40.9	38.2
$n_{\alpha\ helix}$	10.3 ± 0.415	7.81 ± 0.288	9.26 ± 0.0302	14	12	13
β strand (%)	23.2 ± 0.318	30.2 ± 0.731	25.4 ± 0.208	18.5 (14)	22.3	22.3
$n_{\beta\ strand}$	15.4 ± 0.181	18.3 ± 0.582	14.6 ± 0.396	12	12	12
Turn + unordered (%)	48.9 ± 0.503	46.8 ± 0.689	48.7 ± 0.306	41.9 (56)	36.8	39.5
NRMSD	0.0630 ± 0.00900	0.0827 ± 0.0123	0.115 ± 0.00762			
Fold	α/β	α/β	α/β	α/β	α/β	α/β

Secondary structure composition of the BK_{Ca} RCK1 and MthK RCK domains. Deconvolution of far-UV CD spectra performed on the purified WT-RCK1 in the presence and absence of Ca^{2+} and D362/367A-RCK1 into percent secondary structural contributions. The WT-RCK1 domain in 0.00058 µM Ca^{2+} has higher α-helical content than D362/367A-RCK1. The addition of Ca^{2+} to WT-RCK1 changes the secondary structure fractions of the RCK1 domain, decreasing the α-helix content and increasing the β-strand content (see Fig. 6). Secondary structure fractions of the crystallized BK_{Ca} RCK1 domain (Protein Data Bank accession no. 3MT5 estimated from the resolved regions ^{343}KHI...IEY^{570} and ^{577}SRI...YCK^{613}) and the MthK RCK domain in the presence (Protein Data Bank accession no. 1LNQ) or absence (Protein Data Bank accession no. 2FY8) of Ca^{2+} are provided for reference, obtained from the DSSP reference set. Note that the purified RCK1 domain in this study is composed of 346 amino acids (^{322}IIE...HDP^{667}, which amounts to an 81–amino acid difference between the RCK1 domain in this study and the BK_{Ca} RCK1 x-ray structure, and a 126–amino acid difference with respect to the two MthK RCK domains). This region includes the flanking S6-RCK1 linker and part of the RCK1-RCK2 linker, which were not included or resolved in the BK_{Ca} crystal structure. The structure fractions reported in parentheses were estimated by assuming the unresolved RCK1 flaking linker regions possessed no additional α or β structures. Errors represent standard errors of the mean (n = 3). NRMSD, normalized root mean-square deviation.

Folta-Stogniew and Williams, 1999; Philo, 2006) performed on the RCK1 domain in solution confirms its octameric organization. The elution profile of the WT-RCK1 domain is shown in Fig. 3 A. The corresponding mol wt distribution, estimated from light-scattering analysis, is shown superimposed (red circles). A representative Debye plot of light-scattering data with Zimm formalism, taken from the elution slice 2.893 ml, is shown in Fig. 3 B. The inverse of the y-axis intercept of the fit yields a molecular mass of ∼331 kD (Fig. 3 B). A histogram of the relative abundance of mol wts of the eluted protein between volumes 2.6 and 3.3 ml is shown in Fig. 3 C. The majority of eluted WT-RCK1 (76.3%) had mol wts between 316 and 398 kD (mean = 352 ± 24.2 kD). Thus, the purified RCK1 domain preferentially assembles in solution into homo-octamers, similar to bacterial RCK domains (Jiang et al., 2002; Parfenova et al., 2007).

The neutralization of D362 and D367 alters the structure of the RCK1 domain

Within the RCK1 domain, two aspartates (D362 and D367) are critical for the BK_{Ca} channel's Ca^{2+} sensitivity

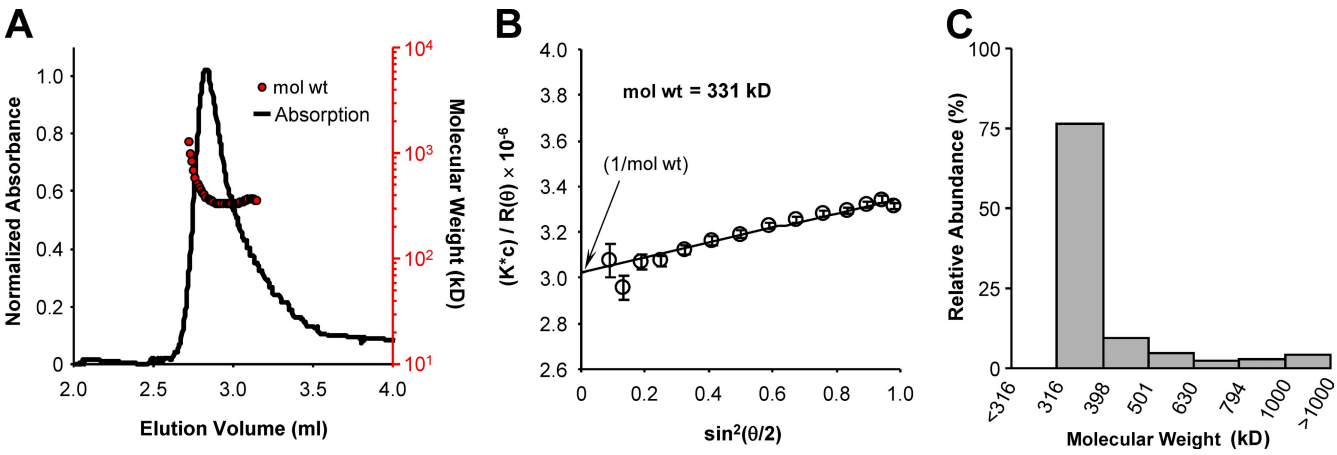

Figure 3. Mol wt determination using MALLS. (A) The normalized absorption at 280 nm (continuous line) of eluted WT-RCK1 is superimposed with its mol wt distribution (red circles) calculated from light-scattering data. (B) A Debye plot with Zimm formalism is shown using the light-scattering data from 14 detectors for the sample at elution volume 2.893 ml. Extrapolation of the fit to zero angle reveals a mean mol wt of eluted protein corresponding to 331 kD. (C) Relative protein abundance (calculated from UV absorbance) of samples eluted between volumes 2.6 and 3.3 ml binned according to mol wt, calculated from MALLS analysis. According to this cumulative distribution, 76.3% of eluted protein had mol wt between 316 and 398 kD, with a mean of 352 ± 24 kD.

in the μM range (Xia et al., 2002; Zeng et al., 2005; Sweet and Cox, 2008). To investigate the structural and functional roles of these residues on RCK1, we introduced mutations D362/367A and probed the secondary structure of the purified D362/367A-RCK1 in solution. Its CD spectrum (shown in Fig. 2 A) is altered as compared with the WT-RCK1 domain. Specifically, a red-shifted minimum from 220 to 223 nm suggests a change in the secondary structure. The analysis of D362/367A-RCK1 CD spectrum reveals that its β content increased from 23 ± 0.3% to 25 ± 0.2%, whereas the α-helix fraction was reduced from 28 ± 0.7% to 25 ± 0.1% compared with WT-RCK1 (Table I). An increase in the β content of proteins has been related to oligomerization (Rotondi and Gierasch, 2006; Zimmer et al., 2006). Interestingly, although WT-RCK1 preferentially self-assembles into an octameric state (Figs. 2, B and C, and 3), we found from size-exclusion chromatography that the D362/367A-RCK1 domain has an apparent mol wt higher than 670 kD (>16-mer). These results suggest that although D362/367A-RCK1 remains soluble and displays an ordered structure, its conformation and oligomeric state are altered.

Time-resolved fluorescence spectroscopy distinguishes between the conformational states of the apo- and Ca^{2+}-bound states of the RCK1 domain

To investigate the Ca^{2+}-dependent properties of the RCK1 domain, we took advantage of the three RCK1 endogenous tryptophan residues (W475/477/524) that can serve as fluorescent probes to resolve possible Ca^{2+}-induced conformational changes. Tryptophan fluorescence lifetime is sensitive to its local environment; therefore, different conformational states of proteins have been reported (Lakowicz, 2006). We used time-correlated single-photon counting spectroscopy to record the excited-state fluorescence lifetime measurements of the endogenous tryptophan residues in the RCK1 domain. The fluorescence intensity decay of WT-RCK1 and D362/367A-RCK1 in the absence and presence of Ca^{2+} are shown in Fig. 4.

The decay of the fluorescence intensity was well fit by the sum of three exponential functions. Mean with standard error fluorescence decay parameters for WT-RCK1 and D362/367A RCK1 in the presence and absence of Ca^{2+} are shown in Table II. The decay of WT-RCK1 fluorescence in the absence of Ca^{2+} (free $[Ca^{2+}]$ = 0.00058 μM) is dominated by the intermediate (τ = 2.0 ± 0.068 ns) and the long-lived components (τ_3 = 5.4 ± 0.049 ns) that have fractional contributions of f_2 = 49% and f_3 = 37% of the total fluorescence intensity, respectively (Table II). The fraction of the shortest-lived component (τ_1 = 0.62 ± 0.040 ns) is f_1 = 14% (n = 3; ±SEM).

In contrast, the WT-RCK1 domain in the Ca^{2+}-bound state (free $[Ca^{2+}]$ = 35 μM) has an intermediate component with a faster time constant of τ_2 = 1.6 ± 0.011 ns and an increased fractional component to f_2 = 65% when

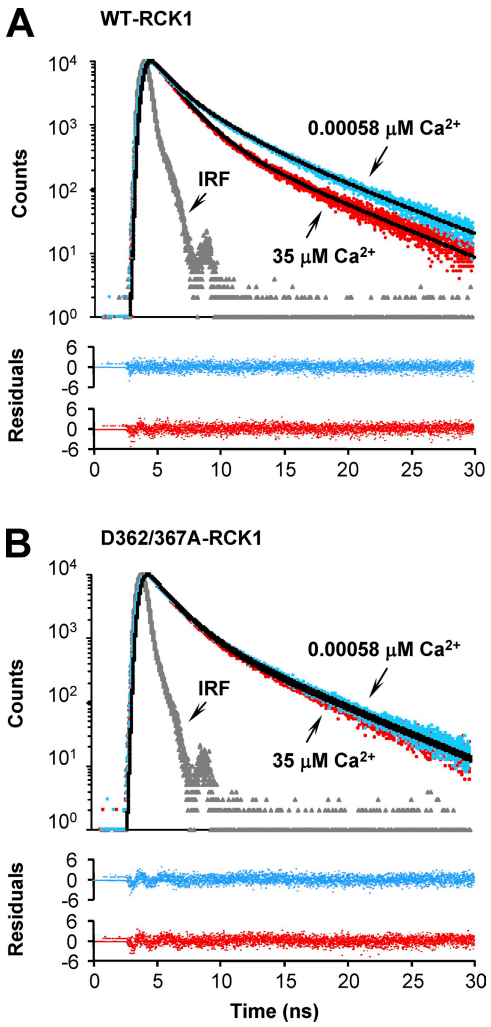

Figure 4. Ca^{2+}-induced conformational changes revealed by the intrinsic tryptophan fluorescence lifetime. Intrinsic tryptophan fluorescence intensity decay of (A) WT-RCK1 and (B) D362/367A-RCK1 recorded in the absence (free $[Ca^{2+}]$ = 0.00058 μM; blue) and presence (35 μM; red) of Ca^{2+}. Black solid curves are the best fit to a triple-exponential decay (Table II). Residuals are shown below the decay curves. The intensity decay of a scattering solution (IRF) is shown in gray. The goodness of the fit was determined from its χ^2 value and the variance of the weighted residual distribution. The triple-exponential analyses gave a χ^2 value close to unity (χ^2 of ~0.86–0.95), whereas fitting the fluorescence decays to the sum of four exponential functions did not improve the accuracy of the fit.

compared with WT-RCK1 in nominal $[Ca^{2+}]$. Furthermore, the time course of the longest-lived component remained practically unchanged (τ_3 = 5.1 ± 0.030 ns), but its fractional contribution decreased to f_3 = 22%. The time course and fractional contribution of the shortest-lived component remained practically unchanged (τ_1 = 0.7 ± 0.018 ns; f_1 = 13%). Also, as shown in Fig. 4 A and Table II, the average excited-state lifetime time constant of the Ca^{2+}-bound protein (free $[Ca^{2+}]$ = 35 μM; τ_{avg} = 2.3 ± 0.067 ns; n = 3) is markedly lower than the *apo*–WT-RCK1 (τ_{avg} = 3.1 ± 0.010 ns), suggesting a

TABLE II

Time-resolved fluorescence lifetime parameters

RCK1	WT		D362/367A	
	$-Ca^{2+}$	$+Ca^{2+}$	$-Ca^{2+}$	$+Ca^{2+}$
τ_1 (ns)	0.62 ± 0.040	0.70 ± 0.018	0.68 ± 0.096	0.71 ± 0.025
τ_2 (ns)	2.0 ± 0.068	1.6 ± 0.011	2.0 ± 0.14	1.9 ± 0.033
τ_3 (ns)	5.4 ± 0.049	5.1 ± 0.030	5.4 ± 0.10	5.4 ± 0.023
α_1	0.42 ± 0.032	0.29 ± 0.020	0.46 ± 0.054	0.45 ± 0.017
α_2	0.45 ± 0.026	0.64 ± 0.018	0.44 ± 0.052	0.45 ± 0.016
α_3	0.12 ± 0.0052	0.068 ± 0.0020	0.10 ± 0.0021	0.10 ± 0.0012
f_1	0.14 ± 0.021	0.13 ± 0.0088	0.18 ± 0.040	0.18 ± 0.013
f_2	0.49 ± 0.011	0.65 ± 0.0062	0.50 ± 0.033	0.50 ± 0.010
f_3	0.37 ± 0.010	0.22 ± 0.0027	0.32 ± 0.0073	0.31 ± 0.0028
τ_{avg} (ns)	3.1 ± 0.010	2.3 ± 0.067	2.8 ± 0.049	2.8 ± 0.0037
χ^2	0.95 ± 0.0053	0.86 ± 0.0092	0.95 ± 0.018	0.95 ± 0.0069

Triple-exponential fitting parameters of fluorescence lifetime. Lifetime fluorescence was recorded at λ_{em} = 330 nm (λ_{ex} = 296 nm). Fractional preexponential factors α_i correspond to lifetimes τ_i, respectively. f_i is fractional contribution of each decay time, and $\tau_{avg} \cdot \chi^2$ values indicate goodness fit. Errors represent standard errors of the mean ($n = 3$).

Ca^{2+}-induced conformational change. On the contrary, the fluorescence lifetime parameters for D362/367A-RCK1 remain similar with the addition of Ca^{2+}, indicating that D362 and D367 are necessary for Ca^{2+} binding, functional transduction of Ca^{2+} binding into conformational rearrangements of the RCK1 domain (Fig. 4 B), or both. We have further explored the effects of these mutations on the Ca^{2+}-sensing properties of RCK1.

Steady-state tryptophan fluorescence reports Ca^{2+}-induced conformational changes in the RCK1 domain

The results from the fluorescence lifetime experiments suggest that the conformational state of RCK1 domain in solution is [Ca^{2+}] dependent (Fig. 4). As BK_{Ca} channels operate in micromolar [Ca^{2+}], we sought to resolve the Ca^{2+} dependence of the observed conformational changes in the following experiments. We recorded changes in steady-state tryptophan fluorescence intensity with increasing [Ca^{2+}] to determine RCK1's apparent affinity for Ca^{2+}. The fluorescence emission spectrum of WT-RCK1 (λ_{ex} = 295 nm) displays a peak at 330 nm, which undergoes significant Ca^{2+}-dependent quenching as the free [Ca^{2+}] is raised from 0.00058 to 35 µM, suggesting the presence of Ca^{2+}-induced conformational rearrangements (Fig. 5 A). On the other hand, the emission spectrum of D362/367A-RCK1 remains practically unchanged up to 35 µM of free [Ca^{2+}] (Fig. 5 B) (similar to albumin, which was used as a negative control), confirming the results from fluorescence lifetime experiments. The apparent Ca^{2+} affinity of RCK1 was estimated by fitting the fluorescence intensity at 330 nm in increasing [Ca^{2+}] to a Hill function. The mean of the parameters of the best fit are: $K_{1/2}$ = 1.7 ± 0.26 µM with n = 1.3 ± 0.19 (n = 3; errors represent standard errors of the mean) (Fig. 5 C).

The results from both time-resolved and steady-state fluorescence experiments are in agreement and provide evidence for the existence of apo- and Ca^{2+}-bound states of the RCK1 domain, revealing Ca^{2+}-induced structural rearrangements of the RCK1 domain occurring in physiologically relevant [Ca^{2+}]. Moreover, evidence is provided that the residues D362 and D367 are required for Ca^{2+}-induced conformational rearrangements.

Ca^{2+}-induced conformational transitions of the BK_{Ca} RCK1 domain

We used CD spectroscopy to characterize the structural changes in terms of the protein's secondary structure. Far-UV CD spectra of the purified WT-RCK1 domain were recorded in increasing [Ca^{2+}] (Fig. 6). As free [Ca^{2+}] was increased from 0.00058 to 35 µM, the CD spectra of WT-RCK1 displayed a decrease in overall molar ellipticity associated to a red shift of the minimum from 220 to 223 nm (Fig. 6 A). The estimated secondary structure fractions of WT-RCK1 plotted as a function of free [Ca^{2+}] are presented in Fig. 6 B. The elevation of free [Ca^{2+}] resulted in an increase of β-strand content (from ∼23 to 30%), accompanied by a decrease in the α-helical fraction (from ∼28 to 19%), whereas the fraction of turns and unordered secondary structures remain practically unchanged (Fig. 6 B and Table I). The apparent Ca^{2+} affinity of the structural transitions was estimated by fitting the α-helical and β-strand fractions with a Hill function ($K_{1/2\_\alpha\text{-helix}}$ = 1.6 ± 0.30 µM; n = 1.4 ± 0.39; and $K_{1/2\_\beta\text{-strand}}$ = 1.2 ± 0.34 µM; n = 1.2 ± 0.04). Intriguingly, the apparent affinity of the Ca^{2+}-dependent structural transitions is in the same range of [Ca^{2+}] relevant to physiological BK_{Ca} channel activation (Bao et al., 2002; Xia et al., 2002; Zeng et al., 2005; Latorre and Brauchi, 2006).

Unlike WT-RCK1, the CD spectrum of D362/367A-RCK1 was practically unaffected by free Ca^{2+} (Fig. 6, C and D) up to 35 µM. This is in agreement with fluorescence spectroscopy experiments and further supports

the premise that residues D362 and D367 are necessary for Ca^{2+}-induced rearrangements in the µM range.

Both WT-RCK1 and D362/367A-RCK1 bind Ca^{2+}

We have presented evidence that RCK1 undergoes Ca^{2+}-induced structural changes and that these conformational rearrangements are no longer detected after the neutralization of residues D362 and D367. An important question is whether these negatively charged aspartates are involved in Ca^{2+} binding. We directly probed the Ca^{2+}-binding properties of both WT-RCK1 and D362/367A-RCK1 (Fig. 7). Both proteins were blotted onto nitrocellulose membranes along with GST and troponin (for negative and positive controls, respectively) and analyzed for $^{45}Ca^{2+}$ binding from 2.1 to 115 µM of free $[Ca^{2+}]$. Fig. 7 A shows a nitrocellulose membrane stained with Ponceau S (for protein quantification) and its corresponding $^{45}Ca^{2+}$ overlay, for 2.1 µM of free Ca^{2+}. Both WT-RCK1 and D362/367A-RCK1 show $^{45}Ca^{2+}$ binding at physiologically relevant $[Ca^{2+}]$, whereas GST displays practically no binding. The ratio of WT- to D362/367A-RCK1 $^{45}Ca^{2+}$ binding is plotted versus free $[Ca^{2+}]$ in Fig. 7 B. Although low-affinity Ca^{2+}-sensing sites E374 and E399 are present in RCK1 (Shi et al., 2002; Zeng et al., 2005; Lingle, 2007; Yang et al., 2007, 2008; Cui et al., 2009), they are unlikely to be responsible for the strong positive $^{45}Ca^{2+}$ signal, as they exhibit Ca^{2+} sensitivity in the mM range (Xia et al., 2002; Zeng et al., 2005).

To exclude the involvement of the N-terminal 6xHis tag (used for purification of the WT-RCK1 domain) in $^{45}Ca^{2+}$ binding, we have enzymatically removed it from the purified protein. Fig. 7 C shows the time-dependent digestion efficiency of the 6xHis tag in WT-RCK1 with DAPase. The $^{45}Ca^{2+}$-binding activity of the 6xHis tag–cleaved WT-RCK1 domain is conserved, as presented in Fig. 7 A. We conclude that the 6xHis tag is not responsible for $^{45}Ca^{2+}$ binding.

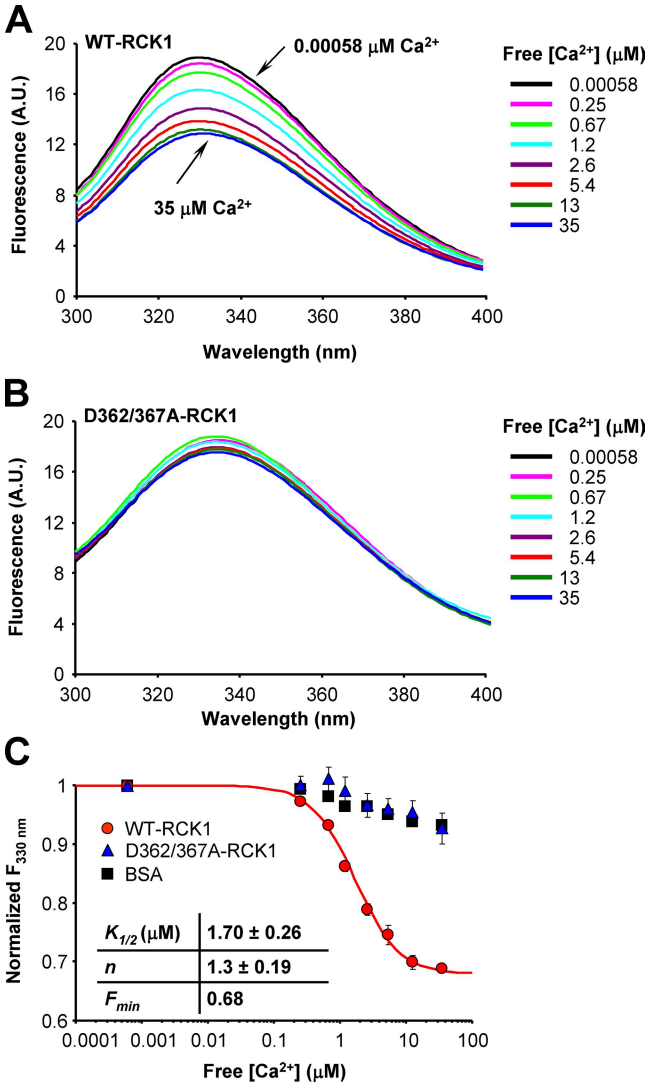

Figure 5. Tryptophan fluorescence reports WT- and D362/367A-RCK1 Ca^{2+} sensitivity. The intrinsic steady-state tryptophan fluorescence emission spectra of (A) WT and (B) D362/367A RCK1 recorded in increasing free $[Ca^{2+}]$. As free $[Ca^{2+}]$ increases, the fluorescence intensity of WT-RCK1 decreases (A), whereas the fluorescence emission of D362/367A (B) shows no significant sensitivity to $[Ca^{2+}]$. (C) The normalized fluorescence intensity at λ_{330nm} and free $[Ca^{2+}] = 0.00058$ µM, plotted against free $[Ca^{2+}]$ for WT-RCK1 (red circles), D362/367A-RCK1 (blue triangles), and albumin (BSA) (black squares). The continuous curve is the least-squares fit to a Hill function, the parameters of which are shown in the panel. Errors represent standard errors of the mean.

DISCUSSION

The human BK_{Ca} RCK1 domain shares structural homology with the bacterial RCK domain

Multiple primary sequence alignments across several species, as well as biochemical and electrophysiological experiments, have suggested that the cytosolic region of the BK_{Ca} channel is composed of two modules termed the RCK1 and RCK2 domains (Jiang et al., 2001, 2002; Pico, 2003; Kim et al., 2006; Latorre and Brauchi, 2006; Yusifov et al., 2008). The x-ray structures of the cytoplasmic domain of the BK_{Ca} channel have confirmed this view and revealed the structural organization of the RCK1 and RCK2 domains, which form a hetero-octameric superstructure referred to as the gating ring (Wu et al., 2010; Yuan et al., 2010). In addition to Ca^{2+}, this intracellular region has been shown to confer sensitivity to other small signaling molecules, such as carbon monoxide (Hou et al., 2008b), Zn^{2+} (Hou et al., 2010), Mg^{2+} (Shi et al., 2002; Yang et al., 2007, 2008), H^+ (Hou et al., 2008a), heme (Tang et al., 2003; Horrigan et al., 2005), and reactive oxygen species (Tang et al., 2004a), which modulate channel activation.

Here, we have probed the structure and investigated the functional properties of the purified BK_{Ca} RCK1 domain in solution under conditions physiologically relevant to the operation of BK_{Ca} channels. In addition to

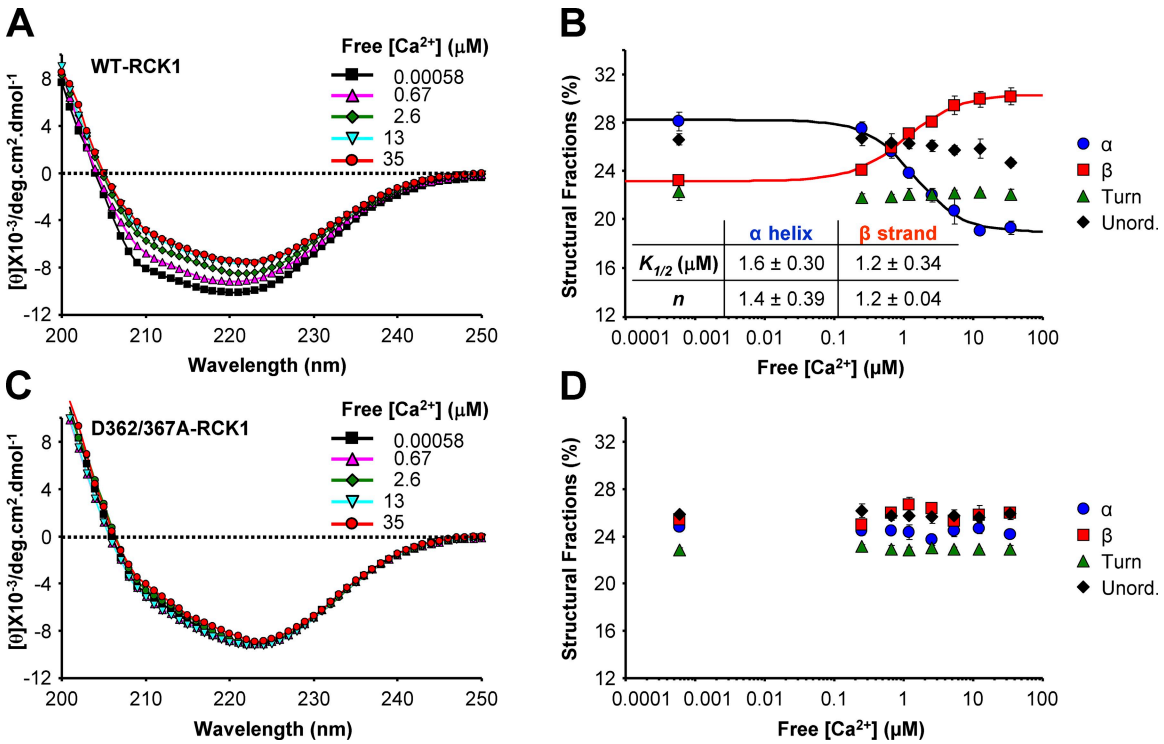

Figure 6. CD spectroscopy reveals Ca^{2+}-dependent conformational changes in the WT-RCK1 domain. (A) Far-UV CD spectra of the BK_{Ca} WT-RCK1 domain obtained in increasing free [Ca^{2+}]. The spectra exhibit decreased overall amplitude with increasing [Ca^{2+}], and a red shift in the ellipticity minimum from 220 to 223 nm, indicating Ca^{2+}-dependent structural alterations. (B) Estimated secondary structure fractions of WT-RCK1 as a function of free [Ca^{2+}]. The α-helix and β-sheet fraction data obtained at different [Ca^{2+}] are fitted to a Hill function. (C and D) As in A and B, respectively, for purified D362/367A-RCK1. The double mutant exhibits little change in secondary structure up to 35 μM of free [Ca^{2+}].

the α/β fold shared with its bacterial counterparts (Jiang et al., 2001, 2002; Yuan et al., 2010), the human RCK1 domains preferentially self-assemble into octameric structures (Figs. 2, B and C, and 3), as observed for RCK domains of MthK and TvoK channels (Jiang et al., 2002; Parfenova et al., 2007). Although RCK1 homo-octamers likely do not occur in functional BK_{Ca} channels, this property of RCK1 domains highlights structural and functional similarities among these ligand-binding domains, emphasizing their significance as modular components of gating ring superstructures. Indeed, the purified human BK_{Ca} RCK2 domain was also found to preferentially self-assemble into octamers (Fig. 8). On the other hand, in the intact BK_{Ca} channel, structurally homologous RCK1 and RCK2 domains can form a hetero-octameric gating ring complex (Wu et al., 2010; Yuan et al., 2010), which likely represents an evolutionary divergence from prokaryotic channel gating rings.

Secondary structure of RCK1 in solution

The RCK1 domain used in this study spans 346 amino acids, including RCK1 flanking regions (S6-RCK1 linker and a portion of the RCK1-RCK2 linker), which are likely unordered. The CD data of this polypeptide obtained under physiological conditions predicted a secondary structure composition of ∼28% α helix and ∼23% β strand (Table I). This region, with the exception of the flanking linkers, was recently resolved at 3-Å resolution (Yuan et al., 2010). The proportion of α-helical structure (considering the unordered RCK1 flanking sections) is in agreement with the CD data (∼30% α-helical structure) (Table I). However the β-strand content in the crystal structure (14%) is reduced compared with the solution structure. Several factors may account for this discrepancy, including differences in experimental conditions (e.g., buffer, pH, and ionic composition); limited resolving power of CD spectroscopy for β strand (Whitmore and Wallace, 2008); and structural changes resulting from the homo-octameric assembly of RCK1 domains.

Ca^{2+}-induced conformational transitions in the RCK1 domain

Here, we have provided evidence that the purified RCK1 domain undergoes Ca^{2+}-induced structural rearrangement. Our steady-state and time-resolved spectroscopic data (Figs. 4 and 5) reveal Ca^{2+}-induced conformational transitions that correlate with an increase in overall β-sheet content (Fig. 6). Although Ca^{2+}-induced structural preference to β sheet has been observed in other proteins (Hilge et al., 2006; Yousefi et al., 2007; Fan et al., 2008), the physiological meaning of this transition in the RCK domains is unknown. Based on the

accepted notion that a gain in β-sheet content (regardless of the cause) may lead to oligomerization or molecular recognition events (Rotondi and Gierasch, 2006; Zimmer et al., 2006), we speculate that in the RCK1 domain, the α-to-β transition may favor or strengthen intra- and/or inter-subunit interactions and possibly the association with other channel partners (Lu et al., 2006). Intriguingly, BK_{Ca} RCK2 domains, where Ca^{2+} binding has been observed in a recent crystal structure (Yuan et al., 2010), also undergo a similar decrease in α/β ratio in solution upon [Ca^{2+}] elevation (Yusifov et al., 2008). Thus, although crystallographic data have not revealed Ca^{2+} binding to BK_{Ca} RCK1, both BK_{Ca} RCK1 and RCK2 domains appear to possess similar Ca^{2+}-sensing properties. It is possible that the RCK1 domain is more likely to bind and respond to Ca^{2+} under conditions resembling those of the cytosolic environment, as those used in this study.

Although Ca^{2+}-induced changes in α/β ratio are exhibited by both BK_{Ca} RCK1 and RCK2 domains, such conformational transitions were not observed in the crystal structures of the MthK RCK domain (Jiang et al., 2002; Ye et al., 2006) (Table I), possibly indicating that gating rings in BK_{Ca} and MthK channels exhibit different Ca^{2+}-dependent activation mechanisms. The large difference in their Ca^{2+} sensitivity, which is three orders of magnitude lower in the MthK channel (Li et al., 2007), may also support this view.

Do D362 and D367 participate in a Ca^{2+}-biding site?

Electrophysiological evidence has highlighted the role of aspartates 362 and 367 in the high-affinity Ca^{2+}-dependent activation of BK_{Ca} channels. Interestingly, residues D362 and D367 have also been shown to be important for the modulation of BK_{Ca} channels by other ligands (Hou et al., 2008a,b); however, the mechanisms by which they exert their function are unknown. The affinity of the putative RCK1 Ca^{2+}-binding site was inferred by allosteric models of BK_{Ca} activation to be ∼1–20 μM (depending on the pore state and the membrane potential) (Bao et al., 2002; Xia et al., 2002; Zeng et al., 2005; Sweet and Cox, 2008; Cui et al., 2009), whereas neutralization of D362/367 reduced it into the millimolar range (Xia et al., 2002). Indeed, this view is recapitulated by the apparent Ca^{2+} sensitivity estimated from steady-state tryptophan fluorescence and CD spectroscopy of the purified WT-RCK1 ($K_{1/2}$ ≈ 1.5 μM Ca^{2+}) and the evidence that D362/367-RCK1 exhibited no response to Ca^{2+}, as no conformational changes were detected up to 35 μM Ca^{2+} (Figs. 4-6). Although it is reasonable to consider their involvement in a Ca^{2+}-binding site, the $^{45}Ca^{2+}$ assay revealed that the neutralization of D362/367 alone was not sufficient to alter the Ca^{2+}-binding activity of RCK1 in the range of 2.1–115 μM of free Ca^{2+} (Fig. 7). The minimal [Ca^{2+}] assayed (2.1 μM) is near the experimental $K_{1/2}$ for the Ca^{2+}-induced conformational changes (Figs. 5 and 6); therefore, conceivably, a change in Ca^{2+} affinity would have been resolved. The data points in Fig. 7 B exhibit a trend that suggests that WT-RCK1 may have slightly higher Ca^{2+} affinity than the mutant; however, statistical significance was not achieved. Thus, WT and mutant RCK1 seem to bind Ca^{2+} with indistinguishable affinity. Collectively, the results favor the hypothesis that D362 and D367 have a major structural role in RCK1, determining their ability to transduce Ca^{2+} binding into conformational rearrangements.

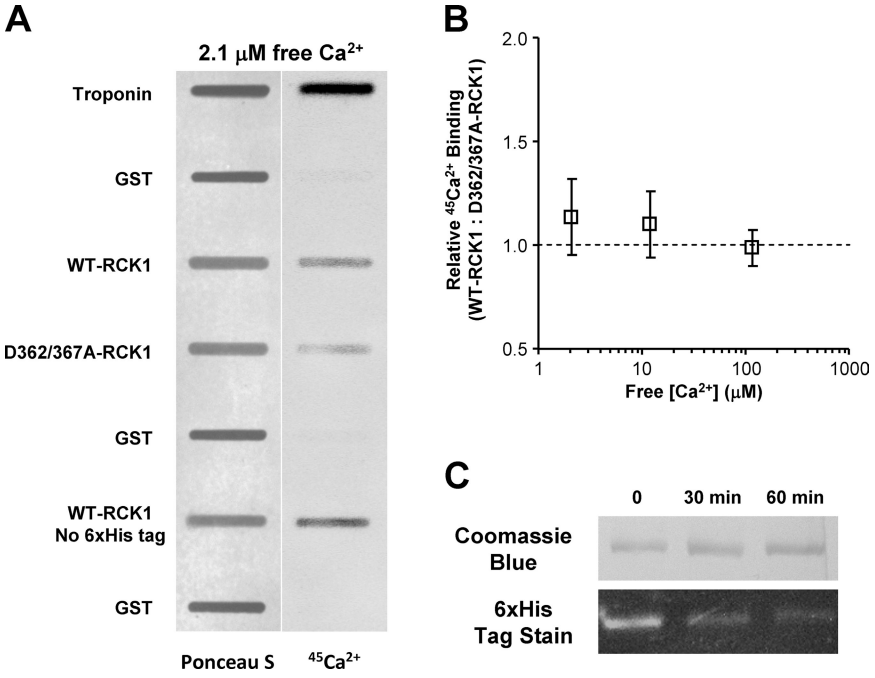

Figure 7. $^{45}Ca^{2+}$ binds to both WT and D362/367A-RCK1 domains. (A) Protein (Ponceau S) staining blotted on nitrocellulose membrane (left) and $^{45}Ca^{2+}$ overlay phosphor image of the same blot (right) in 2.1 μM of free [Ca^{2+}]. Signal intensity is proportional to protein amount (left) and Ca^{2+} binding (right). (B) The ratio of WT to D362/367A-RCK1 Ca^{2+} binding (normalized by protein amount) is plotted versus free [Ca^{2+}]. (C) Enzymatic removal of the 6xHis from the WT-RCK1 domain. The purified 6xHis-WT-RCK1 is incubated with 5 U/ml DAPase, and then separated on a 12.5% SDS-PAGE and stained with either Coomassie Brilliant Blue (top strip) or InVision His tag in-gel stain (Invitrogen) (bottom strip). Troponin and GST are positive and negative controls, respectively. Note that the removal of the histidine tag did not reduce Ca^{2+} binding.

Nevertheless, it cannot be ruled out that D362 or D367 is also an element of a Ca^{2+}-binding site with multiple coordinating residues, so that its neutralization does not substantially impair Ca^{2+} binding. Furthermore, it cannot be excluded that the RCK1 homo-oligomers in solution possess different Ca^{2+}-dependent properties from RCK1 domains incorporated into the BK_{Ca} gating ring, allosterically linked with the pore domain and voltage-sensing apparatus (Horrigan and Aldrich, 2002; Sweet and Cox, 2008).

Structural consequences of D362/367 neutralization

The neutralization of residues D362 and D367 seems to alter the secondary and quaternary structure of the RCK1 domain. The differences in the secondary structure composition of D362/367A-RCK1 relative to the WT are based only on the comparison of the experimental CD data that suggest an increase in β-strand content associated to a decrease in α helix (Fig. 2 A and Table I). CD cannot provide molecular details or information about the region(s) of the protein undergoing this transition, or discriminate between a change occurring in the length of α helices and β strands or in their number, or both. Mutations inducing structural changes that perturb the α/β composition of proteins in solution have been described. For example Ulrih et al. (2008) report a drastic increase in α-helix content after a Tyr>Ala mutation in α synuclein. An Ala>Val mutation greatly increased β-sheet content in N-terminal troponin C (Pinto et al., 2009). In the N-terminal domain of a viral capsid protein, a Pro deletion or Asp>Ala mutation increased the α-helix content by 5% and decreased the β-sheet content by 3–4% (Macek et al., 2009). Increasing the hydrophobicity of residue side chains (as in the D362/367A mutation) can in some cases induce α helix to β-sheet conversion, as reported in a study modeling the energetics of these transitions in simple polypeptides (Imamura and Chen, 2007).

In summary, although a causal relation between the higher β content and loss of Ca^{2+}-induced conformational change is not yet established, the altered structural state of the double mutant retains the ability to bind Ca^{2+} with high affinity but fails to transduce the free energy of ligand association into structural rearrangements. We speculate that in the intact BK_{Ca} channel, these mutations lock RCK1 domains in a conformation state unresponsive to ligand binding, thus hampering the propagation of conformational changes of ligand binding to the gating apparatus.

Both RCK1 and RCK2 are Ca^{2+} sensors with similar biophysical properties

Investigations of the Ca^{2+}-dependent conformational changes of the purified BK_{Ca} RCK1 and RCK2 domains revealed that these two Ca^{2+} sensors exhibit a different Ca^{2+} affinity: RCK1 has less apparent affinity for Ca^{2+} ($K_{1/2} \approx 1.5$ µM) relative to the Ca^{2+} bowl in RCK2 ($K_{1/2} \approx 0.4$ µM) (Yusifov et al., 2008). In spite of this difference, the RCK1 and RCK2 domains share structural similarity (Wu et al., 2010; Yuan et al., 2010). Here, we report that the nature of Ca^{2+}-induced conformational changes of the RCK1 domain are similar to those described for the purified RCK2 domain (Yusifov et al., 2008). Furthermore, the purified RCK2 domain (Fig. 8 A) also preferentially assembles into homomeric octamers in solution (Fig. 8, B and C), similar to RCK1 (Figs. 2, B and C, and 3). Thus, the RCK1 and RCK2 domains share functional and structural similarities.

In summary, we have presented evidence that Ca^{2+}-induced conformational rearrangements take place within the RCK1 region of the BK_{Ca} channel at physiologically relevant [Ca^{2+}]. The Ca^{2+}-dependent properties of this

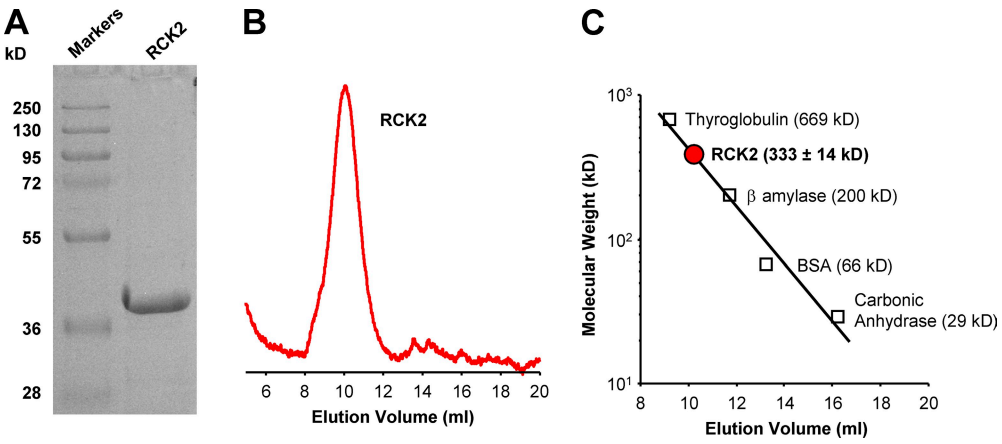

Figure 8. The purified BK_{Ca} RCK2 domain forms a homo-octamer in solution. (A) 12.5% SDS-PAGE analysis of purified RCK2 reveals a single band with a mol wt of ~40 kD, consistent with its expected size (39 kD). (B) Size-exclusion profile of the purified RCK2 domain. RCK2 elutes at 10.15 ml on a Superdex 200 10/300 column. (C) The oligomeric state of the purified RCK2 domain was determined using a calibration curve constructed from protein standards. The purified RCK2 domain corresponds to a mol wt of 333 ± 14 kD ($n = 8$), consistent with a homo-octameric structure of RCK2 (theoretical mol wt = 312 kD). R^2 of fit = 0.97.

structure seem to correlate well with Ca^{2+}-induced BK_{Ca} channel activation. The agreement between the Ca^{2+} dependence of conformational changes (apparent $K_{1/2}$ values obtained from CD and tryptophan fluorescence spectroscopy of ~1.5 μM) with the values obtained from electrophysiological experiments (Bao et al., 2002; Xia et al., 2002; Sweet and Cox, 2008) supports this view. We have demonstrated that the D362/367A mutation, previously shown to impair high-affinity Ca^{2+} sensing (Xia et al., 2002), causes a structural change in the RCK1 domain, preventing Ca^{2+}-dependent conformational rearrangements.

We thank Debora A. Nicoll for her expert advice and assistance; Ligia Toro for the Slo1 clone; Miyeon Kim for MALLS assistance; and Michela Ottolia and the members of the Olcese laboratory for constructive discussions.

This work was supported by National Institutes of Health/National Institute of General Medical Sciences research grant R01GM082289 and the Laubisch Foundation to R. Olcese, and an American Heart Association (Western States Affiliate) Postdoctoral Fellowship to A. Pantazis.

Christopher Miller served as editor.

Submitted: 4 December 2009
Accepted: 28 June 2010

REFERENCES

Bao, L., A.M. Rapin, E.C. Holmstrand, and D.H. Cox. 2002. Elimination of the BK_{Ca} channel's high-affinity Ca^{2+} sensitivity. *J. Gen. Physiol.* 120:173–189. doi:10.1085/jgp.20028627

Bao, L., C. Kaldany, E.C. Holmstrand, and D.H. Cox. 2004. Mapping the BK_{Ca} channel's "Ca^{2+} bowl": side-chains essential for Ca^{2+} sensing. *J. Gen. Physiol.* 123:475–489. doi:10.1085/jgp.200409052

Bian, S., I. Favre, and E. Moczydlowski. 2001. Ca2+-binding activity of a COOH-terminal fragment of the Drosophila BK channel involved in Ca2+-dependent activation. *Proc. Natl. Acad. Sci. USA.* 98:4776–4781. doi:10.1073/pnas.081072398

Braun, A.P., and L. Sy. 2001. Contribution of potential EF hand motifs to the calcium-dependent gating of a mouse brain large conductance, calcium-sensitive K(+) channel. *J. Physiol.* 533:681–695. doi:10.1111/j.1469-7793.2001.00681.x

Carafoli, E., and C.B. Klee. 1999. Calcium As a Cellular Regulator. Oxford University Press, New York. 656 pp.

Chakrapani, S., and E. Perozo. 2007. How to gate an ion channel: lessons from MthK. *Nat. Struct. Mol. Biol.* 14:180–182. doi:10.1038/nsmb0307-180

Clapham, D.E. 1995. Calcium signaling. *Cell.* 80:259–268. doi:10.1016/0092-8674(95)90408-5

Cui, J., H. Yang, and U.S. Lee. 2009. Molecular mechanisms of BK channel activation. *Cell. Mol. Life Sci.* 66:852–875. doi:10.1007/s00018-008-8609-x

Dong, J., N. Shi, I. Berke, L. Chen, and Y. Jiang. 2005. Structures of the MthK RCK domain and the effect of Ca2+ on gating ring stability. *J. Biol. Chem.* 280:41716–41724. doi:10.1074/jbc.M508144200

Fan, D., R. Lakshminarayanan, and J. Moradian-Oldak. 2008. The 32kDa enamelin undergoes conformational transitions upon calcium binding. *J. Struct. Biol.* 163:109–115. doi:10.1016/j.jsb.2008.04.007

Fodor, A.A., and R.W. Aldrich. 2006. Statistical limits to the identification of ion channel domains by sequence similarity. *J. Gen. Physiol.* 127:755–766. doi:10.1085/jgp.200509419

Fodor, A.A., and R.W. Aldrich. 2009. Convergent evolution of alternative splices at domain boundaries of the BK channel. *Annu. Rev. Physiol.* 71:19–36. doi:10.1146/annurev.physiol.010908.163124

Folta-Stogniew, E., and K.R. Williams. 1999. Determination of molecular masses of proteins in solution: implementation of an HPLC size exclusion chromatography and laser light scattering service in a core laboratory. *J. Biomol. Tech.* 10:51–63.

Greenfield, N.J. 2006. Using circular dichroism spectra to estimate protein secondary structure. *Nat. Protoc.* 1:2876–2890. doi:10.1038/nprot.2006.202

Hilge, M., J. Aelen, and G.W. Vuister. 2006. Ca2+ regulation in the Na+/Ca2+ exchanger involves two markedly different Ca2+ sensors. *Mol. Cell.* 22:15–25. doi:10.1016/j.molcel.2006.03.008

Horrigan, F.T., and R.W. Aldrich. 2002. Coupling between voltage sensor activation, Ca^{2+} binding and channel opening in large conductance (BK) potassium channels. *J. Gen. Physiol.* 120:267–305. doi:10.1085/jgp.20028605

Horrigan, F.T., S.H. Heinemann, and T. Hoshi. 2005. Heme regulates allosteric activation of the Slo1 BK channel. *J. Gen. Physiol.* 126:7–21. doi:10.1085/jgp.200509262

Hou, S., R. Xu, S.H. Heinemann, and T. Hoshi. 2008a. Reciprocal regulation of the Ca2+ and H+ sensitivity in the SLO1 BK channel conferred by the RCK1 domain. *Nat. Struct. Mol. Biol.* 15:403–410. doi:10.1038/nsmb.1398

Hou, S., R. Xu, S.H. Heinemann, and T. Hoshi. 2008b. The RCK1 high-affinity Ca2+ sensor confers carbon monoxide sensitivity to Slo1 BK channels. *Proc. Natl. Acad. Sci. USA.* 105:4039–4043. doi:10.1073/pnas.0800304105

Hou, S., L.E. Vigeland, G. Zhang, R. Xu, M. Li, S.H. Heinemann, and T. Hoshi. 2010. Zn2+ activates large conductance Ca2+-activated K+ channel via an intracellular domain. *J. Biol. Chem.* 285:6434–6442. doi:10.1074/jbc.M109.069211

Imamura, H., and J.Z. Chen. 2007. Minimum model for the alpha-helix-beta-hairpin transition in proteins. *Proteins.* 67:459–468. doi:10.1002/prot.21216

Jiang, Y., A. Pico, M. Cadene, B.T. Chait, and R. MacKinnon. 2001. Structure of the RCK domain from the E. coli K+ channel and demonstration of its presence in the human BK channel. *Neuron.* 29:593–601. doi:10.1016/S0896-6273(01)00236-7

Jiang, Y., A. Lee, J. Chen, M. Cadene, B.T. Chait, and R. MacKinnon. 2002. Crystal structure and mechanism of a calcium-gated potassium channel. *Nature.* 417:515–522. doi:10.1038/417515a

Kelly, S.M., T.J. Jess, and N.C. Price. 2005. How to study proteins by circular dichroism. *Biochim. Biophys. Acta.* 1751:119–139.

Kim, H.J., H.H. Lim, S.H. Rho, S.H. Eom, and C.S. Park. 2006. Hydrophobic interface between two regulators of K+ conductance domains critical for calcium-dependent activation of large conductance Ca2+-activated K+ channels. *J. Biol. Chem.* 281:38573–38581. doi:10.1074/jbc.M604769200

Kim, H.J., H.H. Lim, S.H. Rho, L. Bao, J.H. Lee, D.H. Cox, H. Kim, and C.S. Park. 2008. Modulation of the conductance-voltage relationship of the BK Ca channel by mutations at the putative flexible interface between two RCK domains. *Biophys. J.* 94:446–456. doi:10.1529/biophysj.107.108738

Lakowicz, J.R. 2006. Principles of Fluorescence Spectroscopy. 3rd ed. Springer, New York. 954 pp.

Latorre, R., and S. Brauchi. 2006. Large conductance Ca2+-activated K+ (BK) channel: activation by Ca2+ and voltage. *Biol. Res.* 39:385–401. doi:10.4067/S0716-97602006000300003

Latorre, R., C. Vergara, and C. Hidalgo. 1982. Reconstitution in planar lipid bilayers of a Ca2+-dependent K+ channel from transverse tubule membranes isolated from rabbit skeletal muscle. *Proc. Natl. Acad. Sci. USA.* 79:805–809. doi:10.1073/pnas.79.3.805

Levitsky, D.O., D.A. Nicoll, and K.D. Philipson. 1994. Identification of the high affinity Ca(2+)-binding domain of the cardiac Na(+)-Ca2+ exchanger. *J. Biol. Chem.* 269:22847–22852.

Li, Y., I. Berke, L. Chen, and Y. Jiang. 2007. Gating and inward rectifying properties of the MthK K^+ channel with and without the gating ring. *J. Gen. Physiol.* 129:109–120. doi:10.1085/jgp.200609655

Lingle, C.J. 2007. Gating rings formed by RCK domains: keys to gate opening. *J. Gen. Physiol.* 129:101–107. doi:10.1085/jgp.200709739

Lu, R., A. Alioua, Y. Kumar, M. Eghbali, E. Stefani, and L. Toro. 2006. MaxiK channel partners: physiological impact. *J. Physiol.* 570:65–72. doi:10.1113/jphysiol.2005.098913

Macek, P., J. Chmelík, I. Krízová, P. Kaderávek, P. Padrta, L. Zídek, M. Wildová, R. Hadravová, R. Chaloupková, I. Pichová, et al. 2009. NMR structure of the N-terminal domain of capsid protein from the mason-pfizer monkey virus. *J. Mol. Biol.* 392:100–114. doi:10.1016/j.jmb.2009.06.029

Marty, A. 1981. Ca-dependent K channels with large unitary conductance in chromaffin cell membranes. *Nature.* 291:497–500. doi:10.1038/291497a0

Morçöl, T., and A. Subramanian. 1999. A red-dot-blot protein assay technique in the low nanogram range. *Anal. Biochem.* 270:75–82. doi:10.1006/abio.1999.4057

Niu, X., X. Qian, and K.L. Magleby. 2004. Linker-gating ring complex as passive spring and Ca(2+)-dependent machine for a voltage- and Ca(2+)-activated potassium channel. *Neuron.* 42:745–756. doi:10.1016/j.neuron.2004.05.001

Pallotta, B.S., K.L. Magleby, and J.N. Barrett. 1981. Single channel recordings of Ca2+-activated K+ currents in rat muscle cell culture. *Nature.* 293:471–474. doi:10.1038/293471a0

Parfenova, L.V., K. Abarca-Heidemann, B.M. Crane, and B.S. Rothberg. 2007. Molecular architecture and divalent cation activation of TvoK, a prokaryotic potassium channel. *J. Biol. Chem.* 282:24302–24309. doi:10.1074/jbc.M703650200

Philo, J.S. 2006. Is any measurement method optimal for all aggregate sizes and types? *AAPS J.* 8:E564–E571. doi:10.1208/aapsj080365

Pico, A. 2003. RCK domain model of calcium activation in BK channels. PhD thesis. The Rockefeller University, New York. 106 pp.

Pinto, J.R., M.S. Parvatiyar, M.A. Jones, J. Liang, M.J. Ackerman, and J.D. Potter. 2009. A functional and structural study of troponin C mutations related to hypertrophic cardiomyopathy. *J. Biol. Chem.* 284:19090–19100. doi:10.1074/jbc.M109.007021

Pitt, G.S. 2007. Calmodulin and CaMKII as molecular switches for cardiac ion channels. *Cardiovasc. Res.* 73:641–647. doi:10.1016/j.cardiores.2006.10.019

Qian, X., X.W. Niu, and K.L. Magleby. 2006. Intra- and intersubunit cooperativity in activation of BK channels by Ca^{2+}. *J. Gen. Physiol.* 128:389–404. doi:10.1085/jgp.200609486

Rao, S.T., and M.G. Rossmann. 1973. Comparison of super-secondary structures in proteins. *J. Mol. Biol.* 76:241–256. doi:10.1016/0022-2836(73)90388-4

Roosild, T.P., K.T. Lê, and S. Choe. 2004. Cytoplasmic gatekeepers of K+-channel flux: a structural perspective. *Trends Biochem. Sci.* 29:39–45. doi:10.1016/j.tibs.2003.11.008

Rotondi, K.S., and L.M. Gierasch. 2006. Natural polypeptide scaffolds: beta-sheets, beta-turns, and beta-hairpins. *Biopolymers.* 84:13–22. doi:10.1002/bip.20390

Salkoff, L., A. Butler, G. Ferreira, C. Santi, and A. Wei. 2006. High-conductance potassium channels of the SLO family. *Nat. Rev. Neurosci.* 7:921–931. doi:10.1038/nrn1992

Schreiber, M., and L. Salkoff. 1997. A novel calcium-sensing domain in the BK channel. *Biophys. J.* 73:1355–1363. doi:10.1016/S0006-3495(97)78168-2

Schreiber, M., A. Yuan, and L. Salkoff. 1999. Transplantable sites confer calcium sensitivity to BK channels. *Nat. Neurosci.* 2:416–421. doi:10.1038/8077

Sheng, J.Z., A. Weljie, L. Sy, S.Z. Ling, H.J. Vogel, and A.P. Braun. 2005. Homology modeling identifies C-terminal residues that contribute to the Ca2+ sensitivity of a BKCa channel. *Biophys. J.* 89:3079–3092. doi:10.1529/biophysj.105.063610

Shi, J., G. Krishnamoorthy, Y. Yang, L. Hu, N. Chaturvedi, D. Harilal, J. Qin, and J. Cui. 2002. Mechanism of magnesium activation of calcium-activated potassium channels. *Nature.* 418:876–880. doi:10.1038/nature00941

Sreerama, N., and R.W. Woody. 2004. On the analysis of membrane protein circular dichroism spectra. *Protein Sci.* 13:100–112. doi:10.1110/ps.03258404

Sreerama, N., S.Y. Venyaminov, and R.W. Woody. 2001. Analysis of protein circular dichroism spectra based on the tertiary structure classification. *Anal. Biochem.* 299:271–274. doi:10.1006/abio.2001.5420

Sweet, T.B., and D.H. Cox. 2008. Measurements of the BK_{Ca} channel's high-affinity Ca^{2+} binding constants: effects of membrane voltage. *J. Gen. Physiol.* 132:491–505. doi:10.1085/jgp.200810094

Takahashi, A., P. Camacho, J.D. Lechleiter, and B. Herman. 1999. Measurement of intracellular calcium. *Physiol. Rev.* 79:1089–1125.

Tang, X.D., R. Xu, M.F. Reynolds, M.L. Garcia, S.H. Heinemann, and T. Hoshi. 2003. Haem can bind to and inhibit mammalian calcium-dependent Slo1 BK channels. *Nature.* 425:531–535. doi:10.1038/nature02003

Tang, X.D., M.L. Garcia, S.H. Heinemann, and T. Hoshi. 2004a. Reactive oxygen species impair Slo1 BK channel function by altering cysteine-mediated calcium sensing. *Nat. Struct. Mol. Biol.* 11:171–178. doi:10.1038/nsmb725

Tang, X.D., L.C. Santarelli, S.H. Heinemann, and T. Hoshi. 2004b. Metabolic regulation of potassium channels. *Annu. Rev. Physiol.* 66:131–159. doi:10.1146/annurev.physiol.66.041002.142720

Turk, E., O.K. Gasymov, S. Lanza, J. Horwitz, and E.M. Wright. 2006. A reinvestigation of the secondary structure of functionally active vSGLT, the vibrio sodium/galactose cotransporter. *Biochemistry.* 45:1470–1479. doi:10.1021/bi052160z

Ulrih, N.P., C.H. Barry, and A.L. Fink. 2008. Impact of Tyr to Ala mutations on alpha-synuclein fibrillation and structural properties. *Biochim. Biophys. Acta.* 1782:581–585.

Wallner, M., P. Meera, M. Ottolia, G.J. Kaczorowski, R. Latorre, M.L. Garcia, E. Stefani, and L. Toro. 1995. Characterization of and modulation by a beta-subunit of a human maxi KCa channel cloned from myometrium. *Receptors Channels.* 3:185–199.

Wang, L., and F.J. Sigworth. 2009. Structure of the BK potassium channel in a lipid membrane from electron cryomicroscopy. *Nature.* 461:292–295. doi:10.1038/nature08291

Wen, J., T. Arakawa, and J.S. Philo. 1996. Size-exclusion chromatography with on-line light-scattering, absorbance, and refractive index detectors for studying proteins and their interactions. *Anal. Biochem.* 240:155–166. doi:10.1006/abio.1996.0345

Whitmore, L., and B.A. Wallace. 2008. Protein secondary structure analyses from circular dichroism spectroscopy: methods and reference databases. *Biopolymers.* 89:392–400. doi:10.1002/bip.20853

Wu, Y., Y. Yang, S. Ye, and Y. Jiang. 2010. Structure of the gating ring from the human large-conductance Ca(2+)-gated K(+) channel. *Nature.* In press.

Xia, X.M., X. Zeng, and C.J. Lingle. 2002. Multiple regulatory sites in large-conductance calcium-activated potassium channels. *Nature.* 418:880–884. doi:10.1038/nature00956

Yang, H., L. Hu, J. Shi, K. Delaloye, F.T. Horrigan, and J. Cui. 2007. Mg2+ mediates interaction between the voltage sensor and cytosolic

domain to activate BK channels. *Proc. Natl. Acad. Sci. USA*. 104: 18270–18275. doi:10.1073/pnas.0705873104

Yang, H., J. Shi, G. Zhang, J. Yang, K. Delaloye, and J. Cui. 2008. Activation of Slo1 BK channels by Mg2+ coordinated between the voltage sensor and RCK1 domains. *Nat. Struct. Mol. Biol.* 15:1152–1159. doi:10.1038/nsmb.1507

Ye, S., Y. Li, L.P. Chen, and Y.X. Jiang. 2006. Crystal structures of a ligand-free MthK gating ring: insights into the ligand gating mechanism of K+ channels. *Cell.* 126:1161–1173. doi:10.1016/j.cell.2006.08.029

Yousefi, R., M. Imani, S.K. Ardestani, A.A. Saboury, N. Gheibi, and B. Ranjbar. 2007. Human calprotectin: effect of calcium and zinc on its secondary and tertiary structures, and role of pH in its thermal stability. *Acta Biochim. Biophys. Sin. (Shanghai).* 39:795–802. doi:10.1111/j.1745-7270.2007.00343.x

Yuan, P., M.D. Leonetti, A.R. Pico, Y. Hsiung, and R. MacKinnon. 2010. Structure of the human BK channel Ca2+-activation apparatus at 3.0 A resolution. *Science.* In press.

Yusifov, T., N. Savalli, C.S. Gandhi, M. Ottolia, and R. Olcese. 2008. The RCK2 domain of the human BKCa channel is a calcium sensor. *Proc. Natl. Acad. Sci. USA*. 105:376–381. doi:10.1073/pnas.0705261105

Zeng, X.H., X.M. Xia, and C.J. Lingle. 2005. Divalent cation sensitivity of BK channel activation supports the existence of three distinct binding sites. *J. Gen. Physiol.* 125:273–286. doi:10.1085/jgp.200409239

Zimmer, J., W.K. Li, and T.A. Rapoport. 2006. A novel dimer interface and conformational changes revealed by an X-ray structure of B. subtilis SecA. *J. Mol. Biol.* 364:259–265. doi:10.1016/j.jmb.2006.08.044